Controlled Dendrimersome Nanoreactor System for Localised Hypochlorite-Induced Killing of Bacteria

Michael Potter,[†‡] Adrian Najer,[†] Anna Klöckner,[†§] Shaodong Zhang,[†] Margaret N. Holme, [†¥] Valeria Nele,[†] Junyi Che,[†] Lucia Massi,[†] Jelle Penders,[†] Catherine Saunders,[†] James J. Doutch,[♦] Andrew M. Edwards,[§] Oscar Ces,[‡] Molly M. Stevens*[†¥]

[†]Department of Materials, Department of Bioengineering, and Institute of Biomedical Engineering, Imperial College London, London SW7 2AZ, U.K. [‡]Department of Chemistry and Institute of Chemical Biology, Imperial College London, Molecular Sciences Research Hub, London W12 0BZ, U.K. [§]MRC Centre for Molecular Bacteriology and Infection, Imperial College London, London SW7 2AZ, U.K. [¥]Department of Medical Biochemistry and Biophysics, Karolinska Institutet, SE-171 77 Stockholm, Sweden. [♦]ISIS Neutron and Muon Source, STFC, Rutherford Appleton Laboratory, Didcot OX11 ODE, U.K.

Current address: Shaodong Zhang, School of Chemistry and Chemical Engineering, Shanghai Jiao Tong University, Minhang District, Shanghai 200240, China.

*Email: m.stevens@imperial.ac.uk

Supplementary Information

The synthetic procedure of Tris-JD is outlined in Figure S1. Carboxylic acid precursors **2** and **6** were synthesised as described previously.[1] Acetal protected Tris (**1**) was prepared according to a published protocol.[2] Tris-JD was synthesised by the modular attachment of precursors **2** and **6** to the Tris core. The procedures below document the synthesis of intermediates **3**, **4**, **5** and the final compound, Tris-JD. 2-Chloro-4,6-dimethoxy-1,3,5-triazine (CDMT), *N*-methylmorpholine (NMM) and *N,N'*-dicyclohexylcarbodiimide (DCC) were purchased from Sigma. 4-(Dimethylamino)pyridinium 4-toluenesulfonate (DPTS) was prepared according to a previously published protocol.[3]

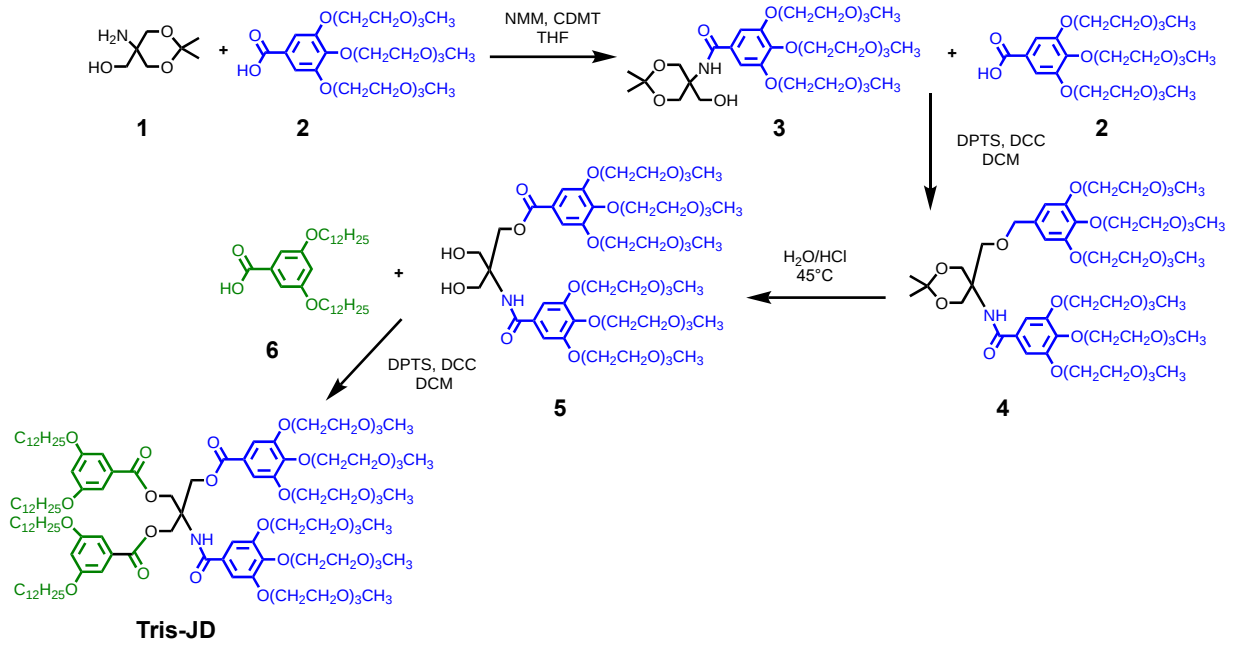

Supplementary Figure 1. Scheme depicting the synthetic route to Tris-JD.

Synthesis of **3**:

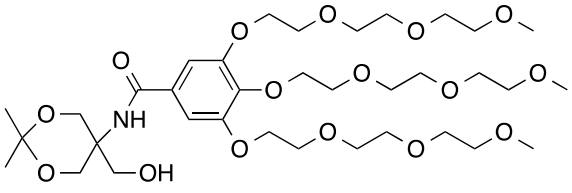

Compound **1** (1.40 mmol, 1 eq.), compound **2** (1.68 mmol, 1.2 eq.) and 2-chloro-4,6-dimethoxy-1,3,5-triazine (2.80 mmol, 2 eq.) were dissolved in anhydrous THF (10 mL). The reaction mixture

was then cooled to 0 ºC and *N*-methylmorpholine (2.80 mmol, 2 eq.) was added dropwise. After stirring overnight at room temperature, de-ionised water (20 mL) was added and the organic phase extracted with DCM (3 x 50 mL). The organic phase was washed with brine (2 x 50 mL), dried with $MgSO_4$ and concentrated in vacuo. The crude product was purified by column chromatography (SiO_2) using an eluent gradient of EtOAc/DCM/MeOH 10:0.5:1 followed by 7:0.5:1 to give the final product as a pale brown oil (56% yield, Rf = 0.13 EtOAc/DCM/MeOH 7:0.5:1). ^{1}H NMR (400 MHz, $CDCl_3$) δ 7.07 (s, 2H), 6.94 (br s, 1H), 4.22-4.19 (m, 6H), 4.04-4.01 (m, 2H), 3.91-3.84 (m, 6H), 3.80-3.78 (m, 4H), 3.73-3.69 (m, 6H), 3.67-3.62 (m, 12H), 3.55-3.51 (m, 6H), 3.37-3.35 (m, 9H), 1.47 (s, 6H).

Synthesis of **4**:

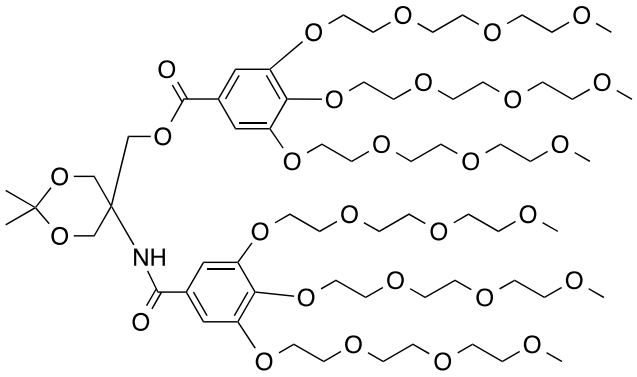

Compound **3** (1.32 mmol, 1.0 eq.), compound **2** (1.98 mmol, 1.5 eq.) and 4-(dimethylamino)pyridinium 4-toluenesulfonate (3.95 mmol, 3.0 eq.) were dissolved in anhydrous DCM (30 mL). To this solution was charged *N*,*N*′-dicyclohexylcarbodiimide (3.95 mmol, 3.0 eq.). After stirring at room temperature overnight a white precipitate formed. De-ionised water (30 mL) was added and the organic phase extracted using DCM (2x100mL), dried using $MgSO_4$ and concentrated in vacuo. The residue was re-dissolved in EtOAc (min. amount) and any residual precipitate filtered on celite. This step was repeated twice. The concentrate was then purified by column chromatography (SiO_2) firstly with DCM, followed by EtOAc/MeOH = 5:1 to give the product as a pale brown oil (47% yield, Rf = 0.16 EtOAc/MeOH 5:1). ^{1}H NMR (400 MHz, $CDCl_3$) δ 7.30 (s, 2H), 7.10 (br s, 1H), 7.04 (s, 2H), 4.82 (s, 2H), 4.65-4.62 (ds, 2H), 4.23-4.15 (m, 12H), 3.88-3.83 (m, 10H), 3.80-3.77 (m, 4H), 3.72-3.69 (m, 12H), 3.66-3.61 (m, 24H), 3.54-3.51 (m, 12H), 3.36-3.35 (m, 18H), 1.60 (s, 3H), 1.47 (s, 3H).

Synthesis of **5**:

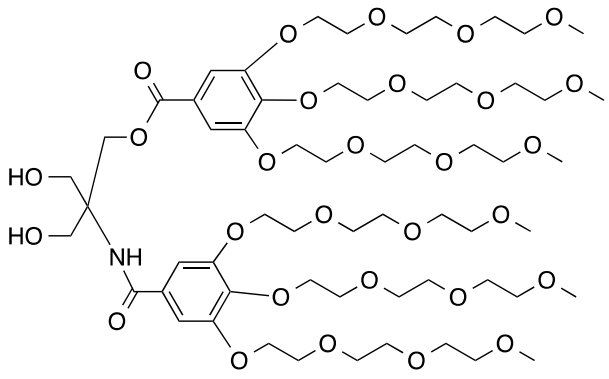

Compound **4** (0.57 mmol) was dissolved in MeOH (20 mL) and the solution warmed to 45 °C. To this solution, Amberlite (8.0 eq., by weight) was added. After stirring for at 45 °C for 5 days the reaction mixture was filtered on celite. The filtrate was concentrated in vacuo to give the final product as a pale brown oil (yield 96%, Rf = 0.26 EtOAc/MeOH 1:1). ^{1}H NMR (400 MHz, $CDCl_3$) δ 7.31 (s, 2H), 7.10 (s, 2H), 4.64 (s, 2H), 4.24-4.17 (m, 12H), 3.88-3.83 (10H), 3.80-3.77 (m, 4H), 3.74-3.69 (m, 14H), 3.67-3.61 (m, 24H), 3.55-3.51 (m, 12H), 3.37-3.35 (m, 18H).

Synthesis of **Tris-JD**:

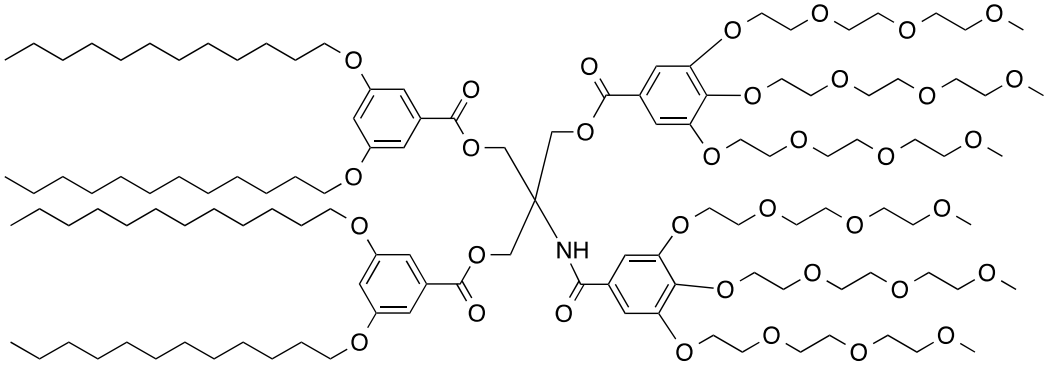

Compound **5** (0.56 mmol, 1.0 eq.) compound **6** (1.41 mmol, 2.5 eq.) and 4-(dimethylamino)pyridinium 4-toluenesulfonate (2.25 mmol, 4.0 eq.) were dissolved in anhydrous DCM (20 mL). To this *N*,*N′*-dicyclohexylcarbodiimide (2.25 mmol, 3 eq.) was added. After stirring at room temperature overnight the reaction mixture was filtered on celite and the filtrate concentrated in vacuo. The residue was re-dissolved in EtOAc (min. amount) and any residual precipitate was filtered on celite. This step was repeated twice. The concentrate was purified by column chromatography (SiO_2) with DCM/EtOAc/MeOH = 5:5:1 to give the final product as a light brown/off-white oil (yield 72%, Rf = 0.44 DCM/EtOAc/MeOH 5:5:1). ^{1}H NMR (400 MHz,$CDCl_3$) δ

7.42 (s, 1H), 7.24 (s, 2H), 7.08 (d, *J* = 2.3 Hz, 4H), 7.04 (s, 2H), 6.60 (t, *J* = 2.3 Hz, 2H), 5.00-4.93 (m, 6H), 4.21-4.16 (m, 8H), 4.12-4.09 (m, 4H), 3.88 (t, *J* = 6.5 Hz, 8H), 3.85-3.81 (m, 8H), 3.80-3.77 (m, 4H), 3.73-3.69 (m, 12H), 3.66-3.60 (m, 24H), 3.54-3.50 (m, 12H), 3.37-3.34 (m, 18H), 1.77-1.70 (m, 8H), 1.44-1.38 (m, 8H), 1.34-1.24 (m, 64H), 0.87 (t, *J* = 6.7 Hz, 12H). ^{13}C NMR (101 MHz, $CDCl_3$) δ 167.14, 166.62, 166.29, 160.32, 152.62, 152.48, 143.23, 141.51, 131.00, 129.07, 124.07, 110.11, 109.27, 107.91, 106.78, 106.49, 72.55, 72.04, 70.90, 70.78, 70.65, 69.73, 69.02, 68.92, 68.45, 64.15, 64.10, 60.09, 59.13, 32.05, 29.83, 29.78, 29.74, 29.58, 29.49, 29.33, 26.19, 22.82, 14.26. MALDI-TOF (m/z) calcd. $[M+Na]^+$ for $C_{122}H_{207}NO_{35}$, 2270.97, found 2270.60.

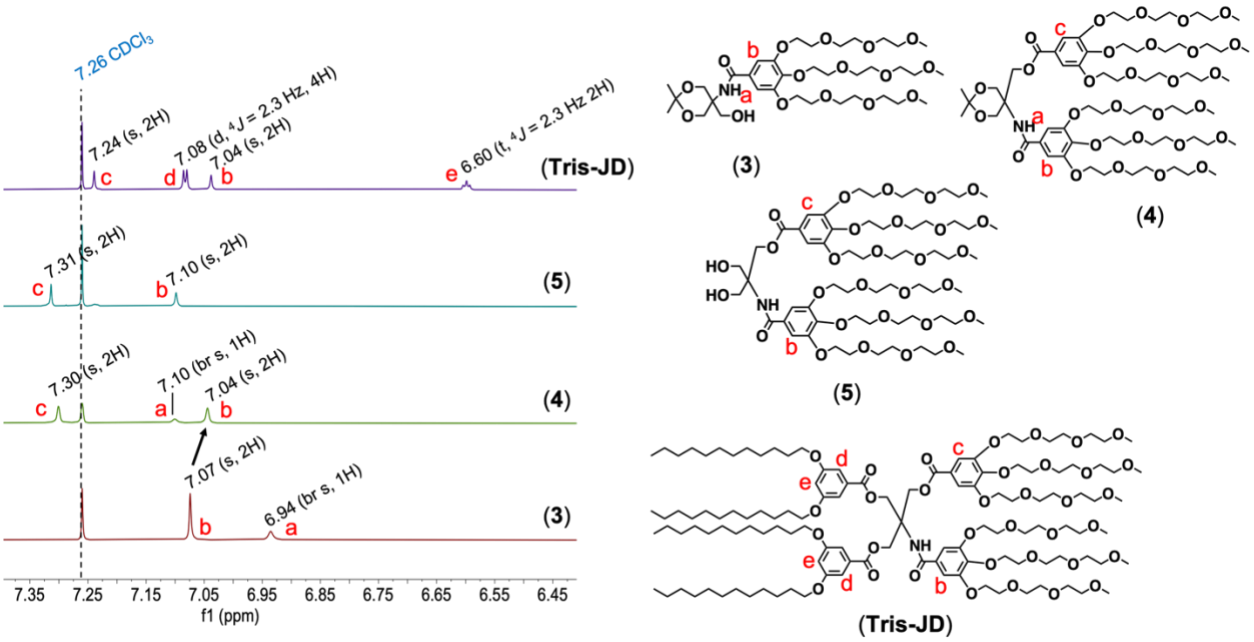

Supplementary Figure 2. ^{1}H NMR analysis of modular dendron attachment to acetal protected Tris. Figure shows stacked aromatic regions (7.35 – 6.45 ppm) of the ^{1}H NMR spectrum for intermediates 3, 4, 5 and the final dendrimer Tris-JD. Sequential addition of dendrons was tracked by stepwise changes in the aromatic region of the NMR spectrum. Protons c and d exhibit ^{4}J coupling constants. Tris-JD exhibits a shift (not shown in this figure) at 7.42 (s, 1H) attributed here to the amide proton (which is also observed in ^{1}H NMR of 3 and 4).

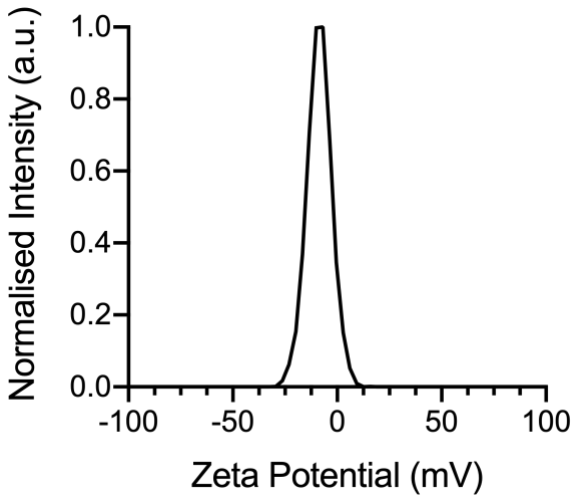

Supplementary Figure 3. Zeta potential distribution for DS. Mean ± SD = -9.2 ± 5.9 mV (N =1, n = 3).

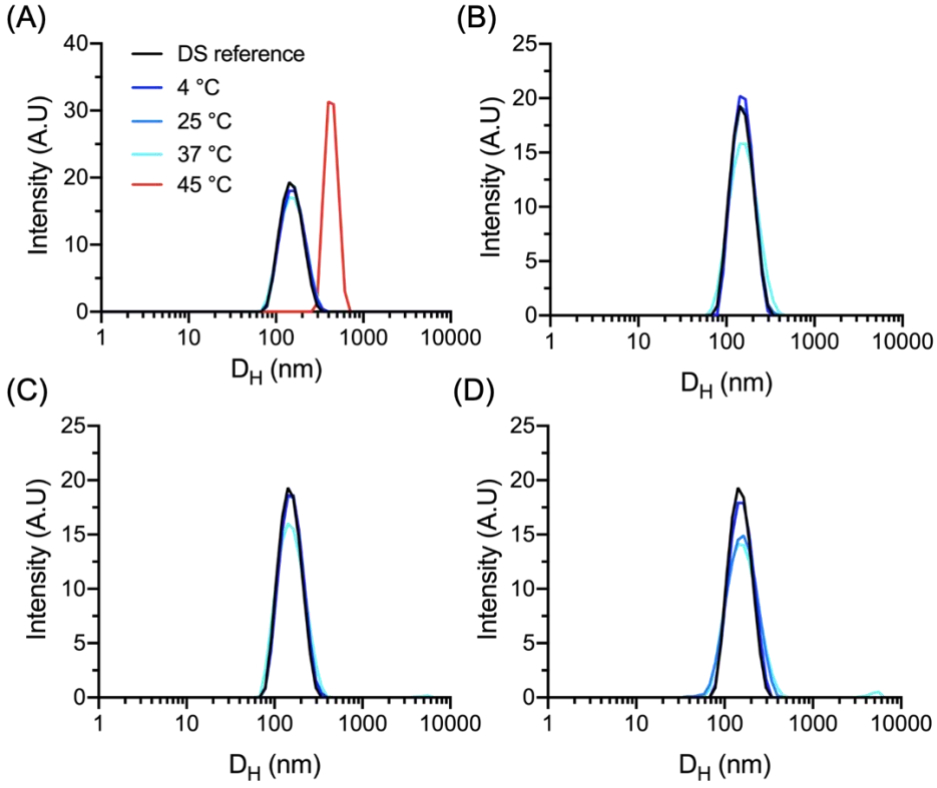

Supplementary Figure 4. Stability of DS in DPBS incubated at various temperatures for (A) 5 hours (B) 2 days, (C) 7 days and (D) 11 days post assembly. DS reference represents the DLS trace measured immediately post fabrication.

Raman shift (cm^{-1})	Ref. Raman shift[4] (cm^{-1})	Vibration (Assignment)
736	728	*C-C* stretch
848	847	*C-O-C* skeletal
893	893	*C-C* skeletal
994	1000-1005	*C-C* (aromatic ring) stretch
1028	1029	*O-*CH_3 stretch
1058	1053, 1060-1064	*C-O, C-N* or *C-C* stretch (overlap)
1128	1128	*C-N* or *C-O* stretch
1242	1243	Amide
1302	1296-1314	CH_2 twist
1340	1339	*C-C* (phenyl) stretch
1453	1442-1450	CH_2 bend
1596	1583, 1600-1607	*C=C* (phenyl) bend
1666	1667-1669	*C=O* stretch
1723	1710-1740	*C=O* (ester) stretch

Supplementary Table 1. Raman spectral assignment of DS. Raman spectrum from SPARTA® experiment can be found in Figure 1 of the main text. Full spectral assignment was made using published values.[4]

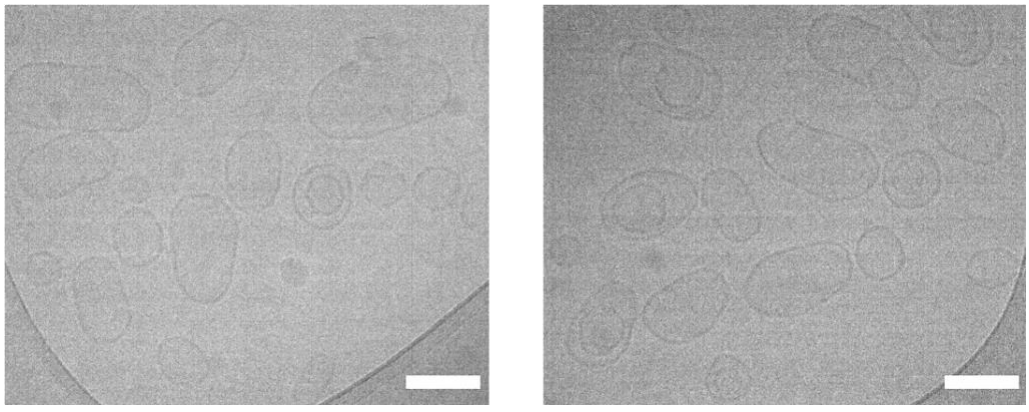

Supplementary Figure 5. Additional cryo-TEM images of DSs formed from Tris-JD. Scale bars = 100 nm.

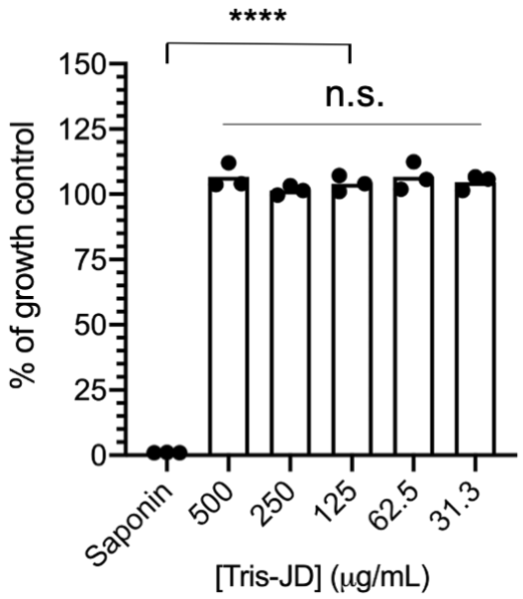

Supplementary Figure 6. Cytotoxicity of DS to HepG2 cells. Cells were viable to all tested concentrations of Tris-JD. Bars represent mean values (N = 3, n = 3). Each dot represents the mean average of each biological repeat. Statistical test used: One-way ANOVA with Tukey's multiple comparisons test, with a single pooled variance. $P < 0.05$ was considered to be statistically significant; ****$P < 0.0001$).

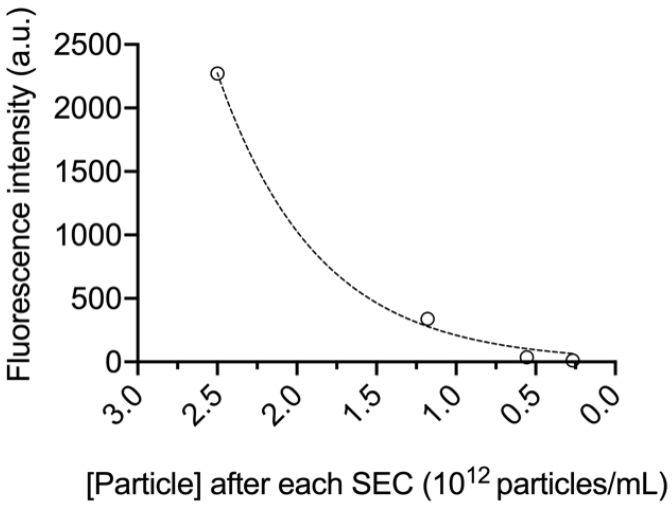

Supplementary Figure 7. Exponential decrease of SRB fluorescence observed for DS during sequential SEC process (zoom-in of data shown in Fig. 2B).

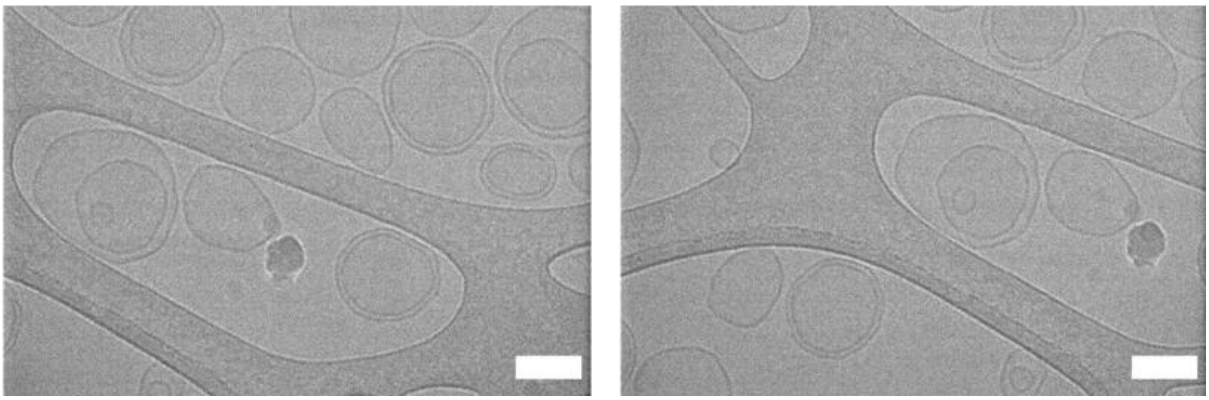

Supplementary Figure 8. Cryo-TEM images of DS self-assembled in the presence of OG-HRP. Scale bars = 100 nm.

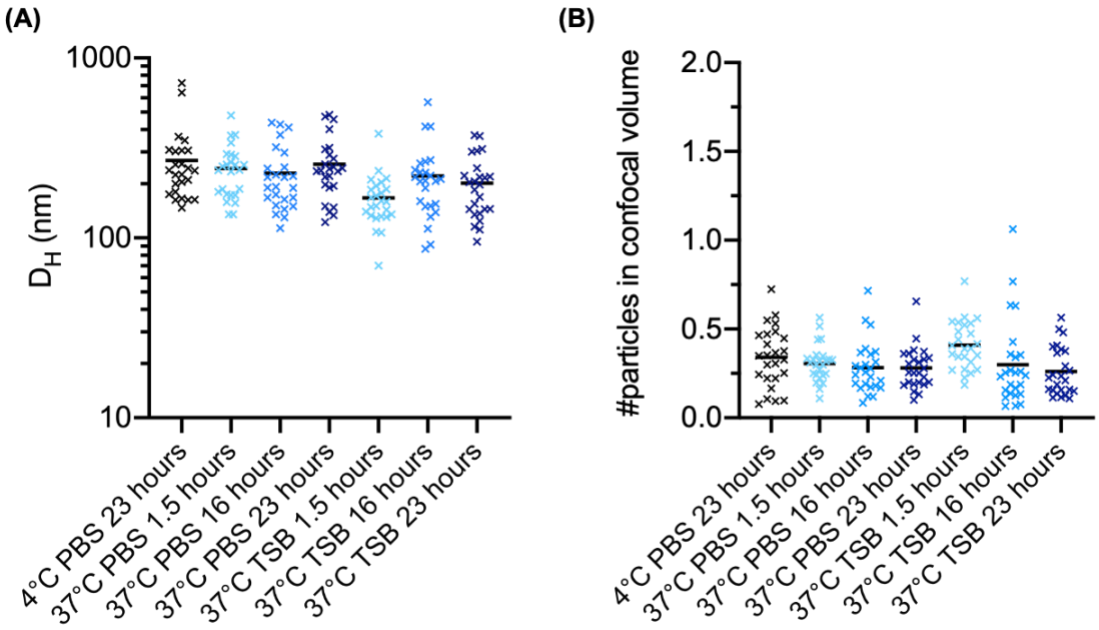

Supplementary Figure 9. FCS assessment of EMP-DS-DiD stability at 37 °C in DPBS and TSB**.** (A) and (B) are plots of EMP-DS-DiD size (D_H) and particle number. Both show EMP-DS-DiD is stable to aggregation and particle degradation over a period of 23 hours in DPBS and TSB (N = 1, n = 25).

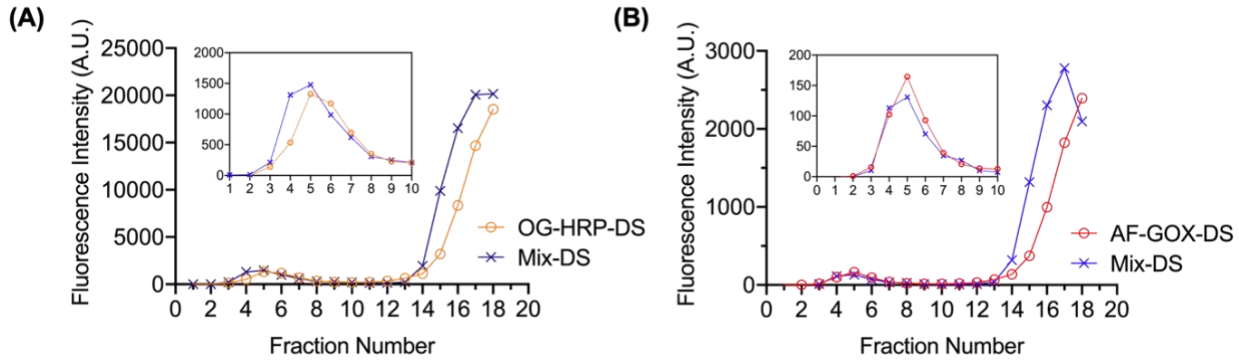

Supplementary Figure 10. SEC plots (A) for OG-HRP-DS and Mix-DS measured at 526 nm and (B) for AF-GOX-DS and Mix-DS at 670 nm.

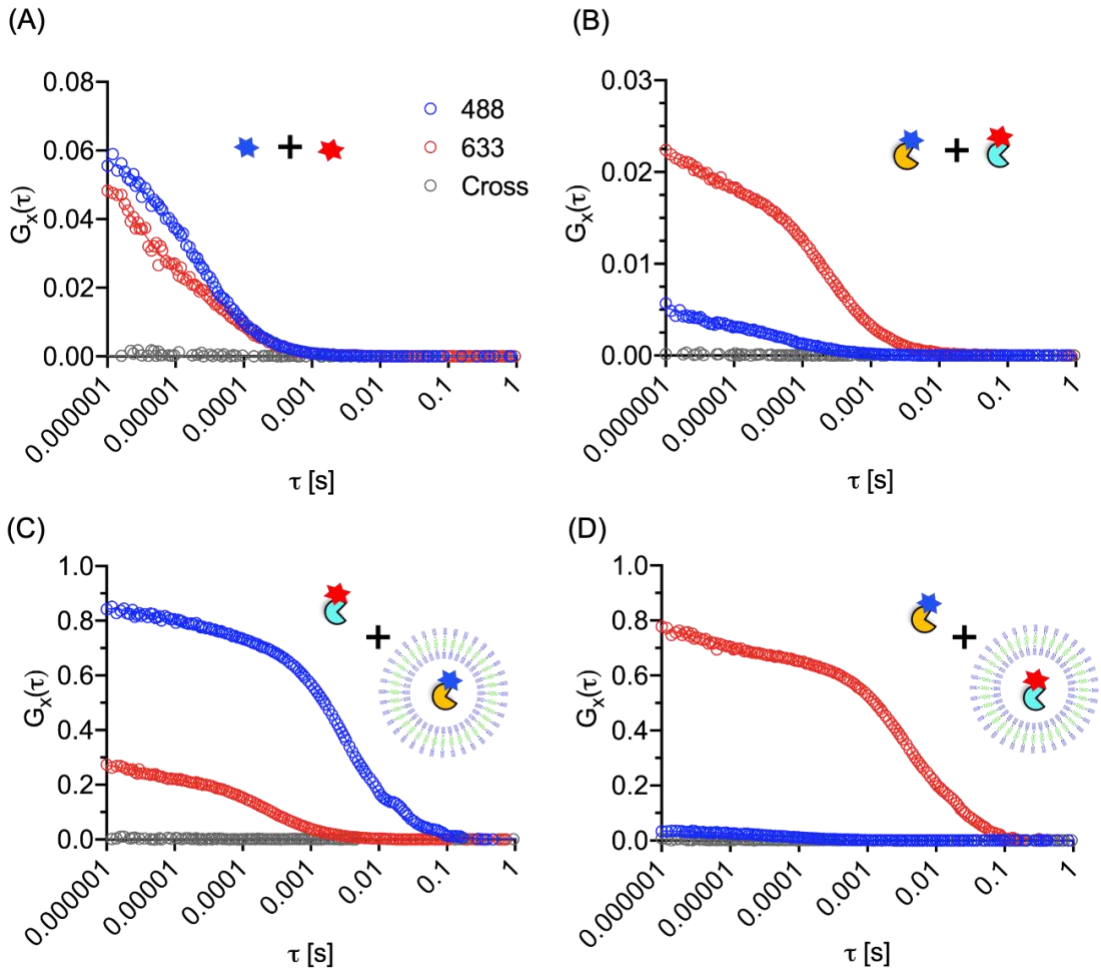

Supplementary Figure 11. FCS autocorrelation and FCCS cross-correlation curves measured in the 488 nm, 633 nm and cross channels for (A) free dyes mixed (OG + AF) (B) free proteins mixed (OG-HRP + AF-GOX) (C) OG-HRP-DS + AF-GOX and (D) AF-GOX-DS + OG-HRP.

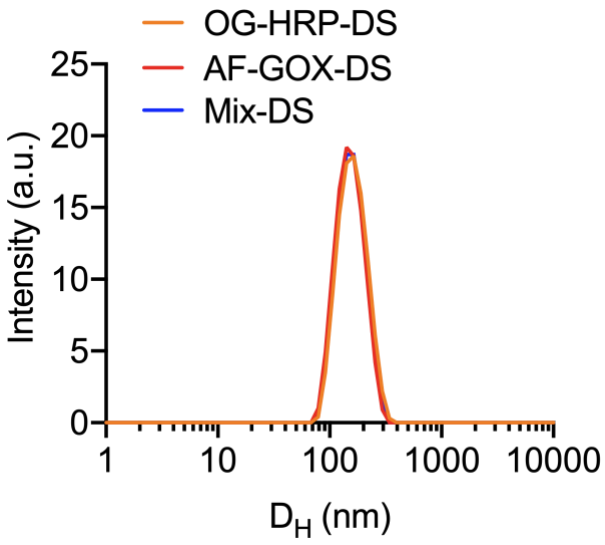

Supplementary Figure 12. DLS traces (intensity distribution) of OG-HRP-DS, AF-GOX-DS and Mix-DS.

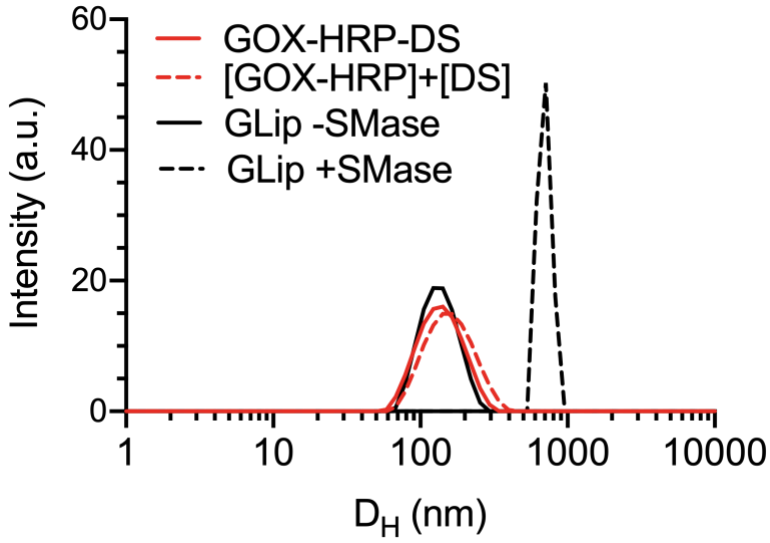

Supplementary Figure 13. DLS traces of GOX-HRP-DS, [GOX-HRP]+[DS], GLip -SMase and GLip +SMase. The latter exhibits aggregation consistent with the activity of SMase upon its membrane.

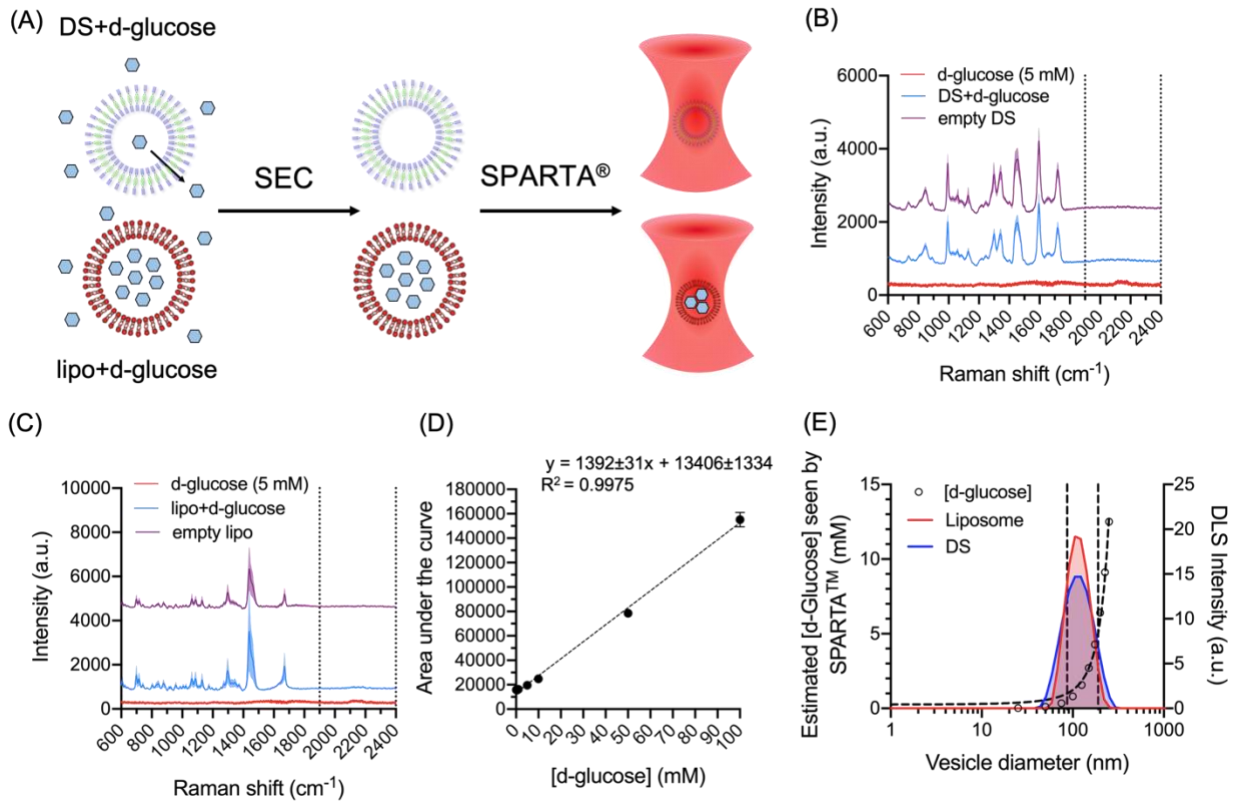

Supplementary Figure 14. Supplementary SPARTA® data for demonstration of DS glucose permeability. (A) DS and BSM:CH liposomes prepared in the presence of 300 mM d-glucose in H_2O. Prepared vesicles were purified by SEC in isotonic conditions followed by population analysis using SPARTA®. Glucose permeates from within DS and thus cannot be detected by SPARTA®. (B, C) Mean non-normalised Raman spectrum (offset) of DS and BSM:CH liposomes prepared with and without 300 mM d-glucose (5 mM d-glucose included in both plots for reference). Shaded region shows the standard deviation and dotted line represents the magnified Raman shift region in Fig. 3I and 3J. (D) Calibration curve of free d-glucose in the SPARTA® confocal volume. Data are mean ± SD (n = 20). (E) Comparison of theoretical [d-glucose] that would be observed by SPARTA® for a given vesicle diameter and DLS traces (intensity distributions) measured for DS and BSM:CH liposomes. Black circles represent estimated [d-glucose] concentrations that would be observed by SPARTA® for a given vesicle diameter and estimated confocal volume. Points were fitted to an exponential growth equation; y = 0.258*exp(0.016*x). Black dashed lines mark the region of particle sizes that would equate to between 1 – 5 mM d-glucose (a range covering 3.6 ± 1.0 mM measured for lipo+d-glucose) in the SPARTA® confocal volume (calculated from the theoretical exponential fit). Overlaid DLS traces for the DS and liposomes overlap well with each other, and the marked size range, illustrating the compartmentalisation of d-glucose in the liposomes and permeation from the DS.

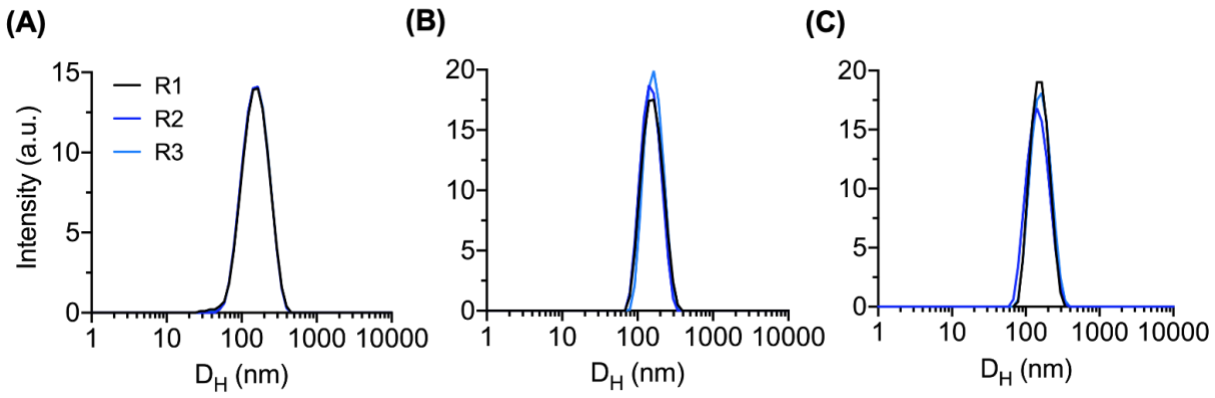

Supplementary Figure 15. DLS traces (intensity distributions) of 3 repeat particle batches for (A) EMP-DS (163 ± 62 nm; 163 ± 62 nm; 163 ± 64 nm) (B) GOX-DS (169 ± 47 nm; 156 ± 45 nm; 164 ± 50 nm) and (C) GOX-MPO-DS (166 ± 50 nm; 153 ± 50 nm; 160 ± 45 nm).

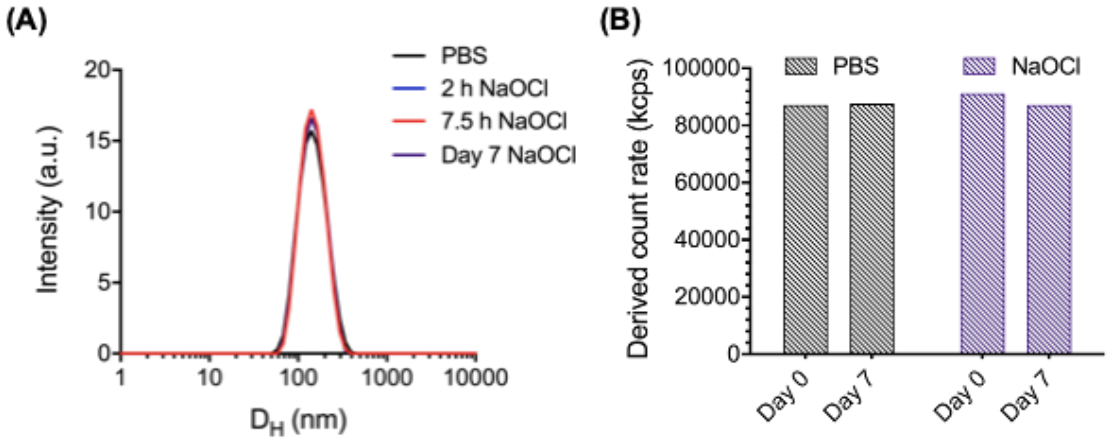

Supplementary Figure 16. (A) DLS traces (intensity distribution) for EMP-DS incubated in 2% (*v:v*) NaOCl over a 7 day period. (B) Corresponding derived count rate of EMP-DS in the absence and presence of 2% (*v:v*) NaOCl. Data shown as mean (n = 2).

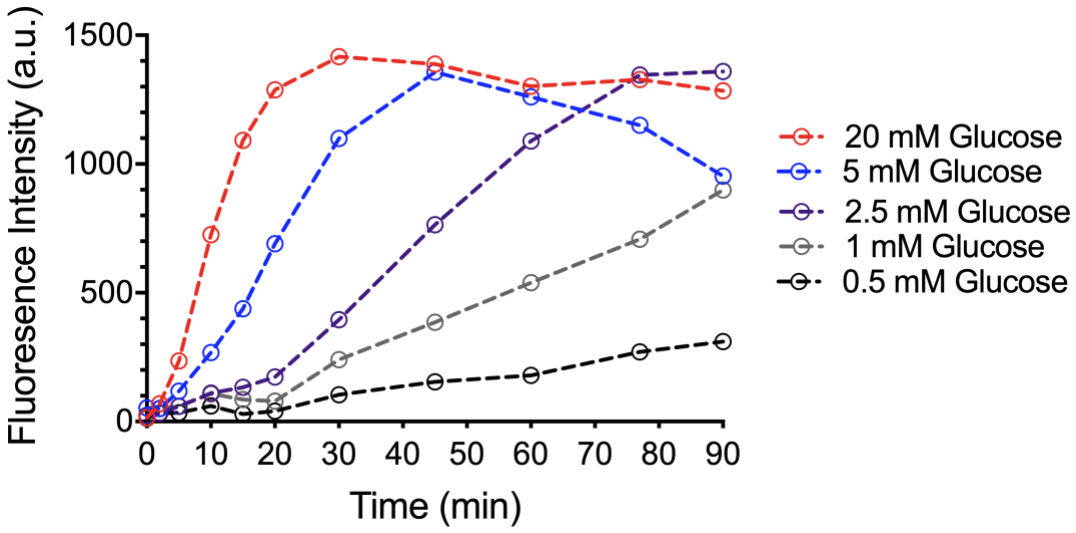

Supplementary Figure 17. Fluorescence *vs*. time graph to show production of $^{-}$OCl by GOX-MPO-DS down to a concentration of 0.5 mM glucose. Data shown as mean (n = 2). Lines are included as a guide for the eye.

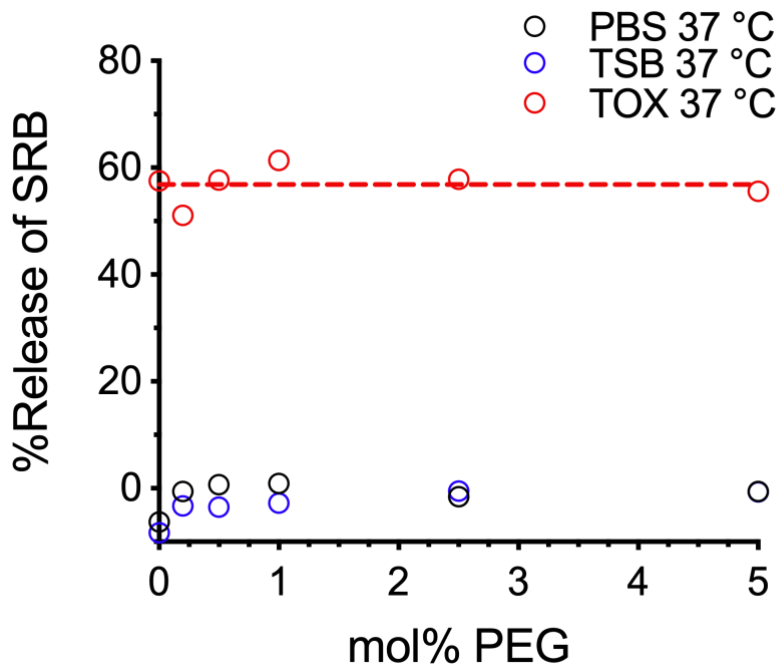

Supplementary Figure 18. Incubation of *S. aureus* Je2 culture supernatants (TOX) with BSM:CH (50:50 w:w) LUVs containing SRB at 37 °C for 2 hours. Liposomes were mixed with bacteria cell culture media (TSB) or PBS as controls. Liposomes tested contained varying mol% of DSPE-PEG2K with respect to moles of BSM. PEG = DSPE-PEG2K.

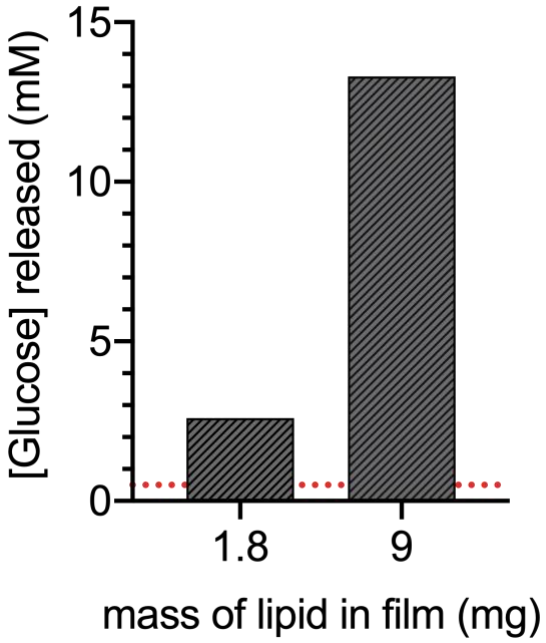

Supplementary Figure 19. Quantification of released glucose from GUVs following 2 hours incubation with Tox using SRB as a fluorescent marker. GUVs were prepared using two different concentrations of initial lipid in the hydration (1.8 and 9 mg mL^{-1}). Red dotted line represents lowest concentration tested to switch on GOX-MPO-DS in Supplementary Figure 17.

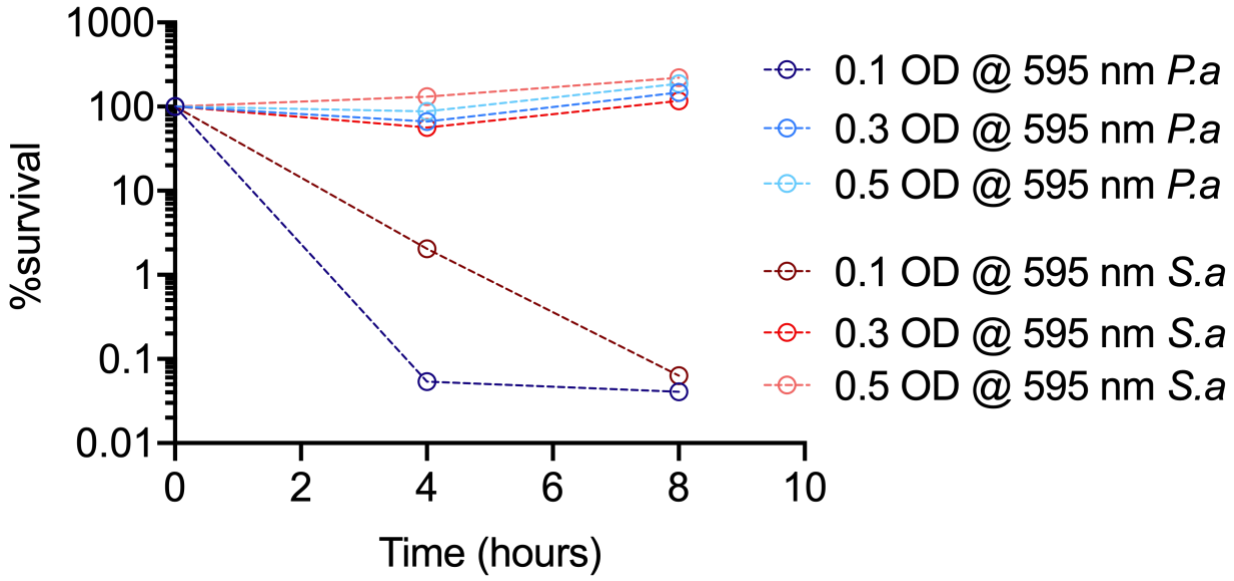

Supplementary Figure 20. Effect of bacteria concentration on reactor efficacy. Percentage survival plots of *S. aureus* JE2 (*S.a*) and *P. aeruginosa* PA14 (*P.a*) at varying initial OD_{595} (concentration) incubated with GOX-MPO-DS and 20 mM glucose for 8 hours (N = 1, n = 1). Lines are included as a guide for the eye. Data shows no bactericidal effect at OD = 0.3 or 0.5 for either bacteria strain.

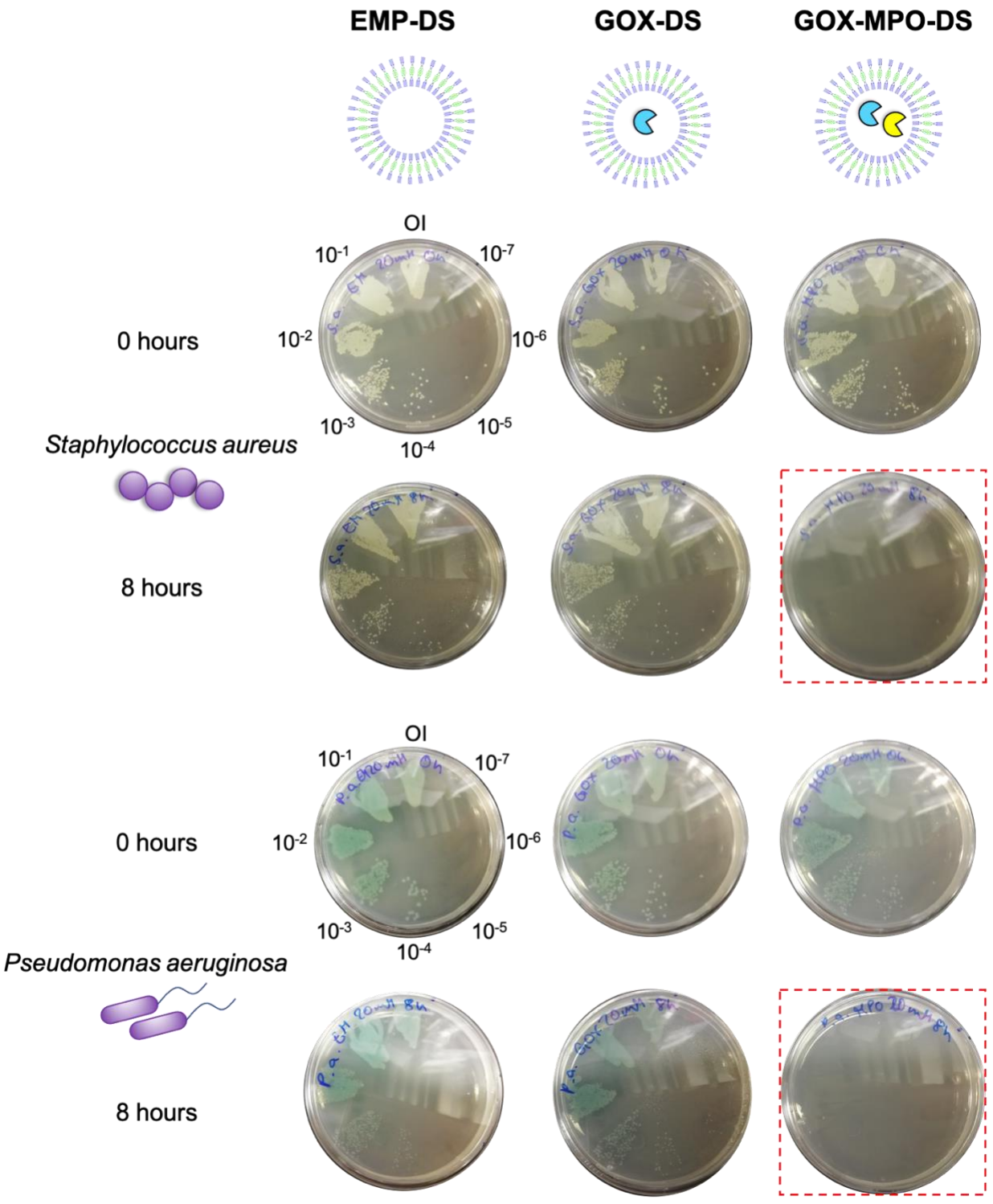

Supplementary Figure 21. Representative agar plates used for CFU counting assessment of DS nanoreactor bactericidal effect. Data shows agar plates for *S. aureus* (JE2) and *P. aeruginosa* (PA14) treated with 20 mM glucose at 0 and 8 hours incubation times. Red marked plates show complete elimination of viable bacteria in the original inoculum. Bacteria were diluted to 10^{-7} of the original inoculum for CFU counting.

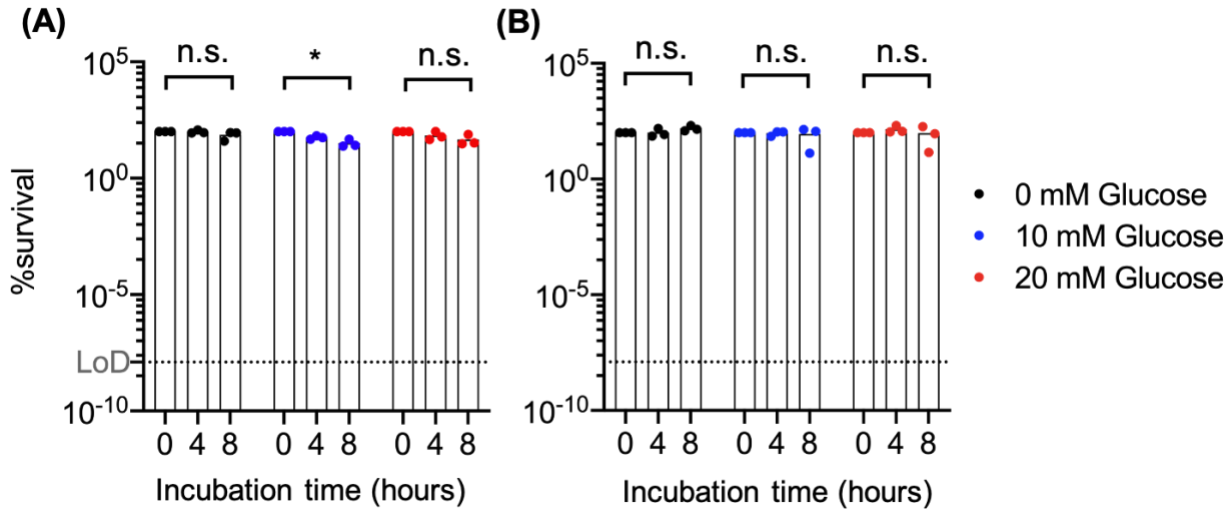

Supplementary Figure 22. Survival plots of (A) *S. aureus* JE2 and (B) *P. aeruginosa* PA14 following incubation with EMP-DS, glucose (0, 10, 20 mM) and NaCl (137 mM). LoD = 1.25×10^{-8} %. Bars represent mean (N = 3, n = 1). Dots represent each biological repeat. Statistical significance was determined using a two-way ANOVA with Geisser-Greenhouse correction with Tukey's multiple comparisons test. $P < 0.05$ was considered to be statistically significant.

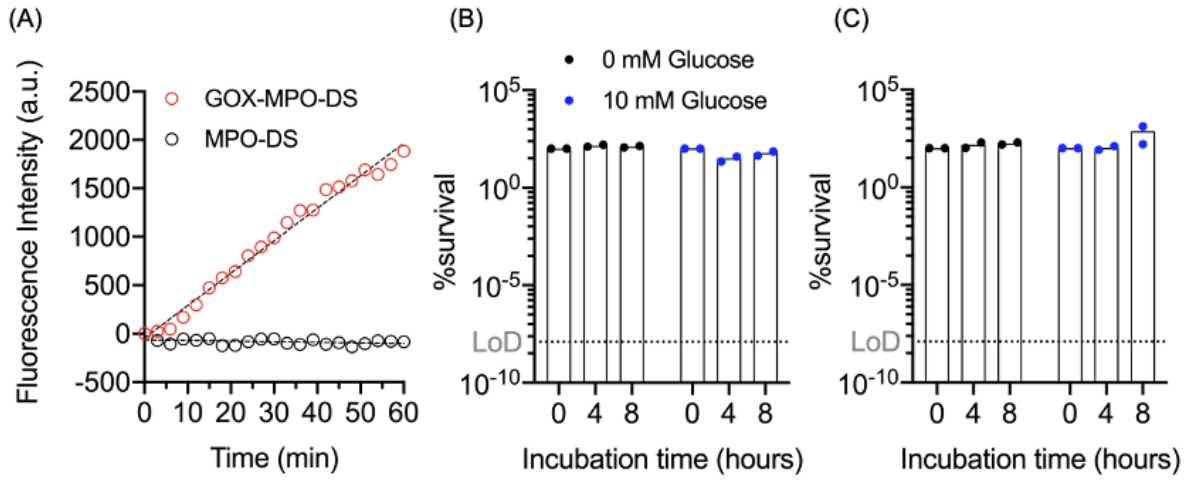

Supplementary Figure 23. Bactericidal effect of MPO-DS against *S. aureus* Je2 and *P. aeruginosa* PA14. (A) APF assay of MPO-DS in the presence of glucose (20 mM) and NaCl (137 mM). No $^{-}$OCl production was detected in comparison to GOX-MPO-DS. Data shown as mean (n = 2). (B) and (C) are survival plots of *S. aureus* JE2 and *P. aeruginosa* PA14 following incubation with MPO-DS, glucose (0, 10 mM) and NaCl (137 mM). LoD = 1.25×10^{-8} %. Bars represent mean (N = 2, n = 1). Dots represent each biological repeat.

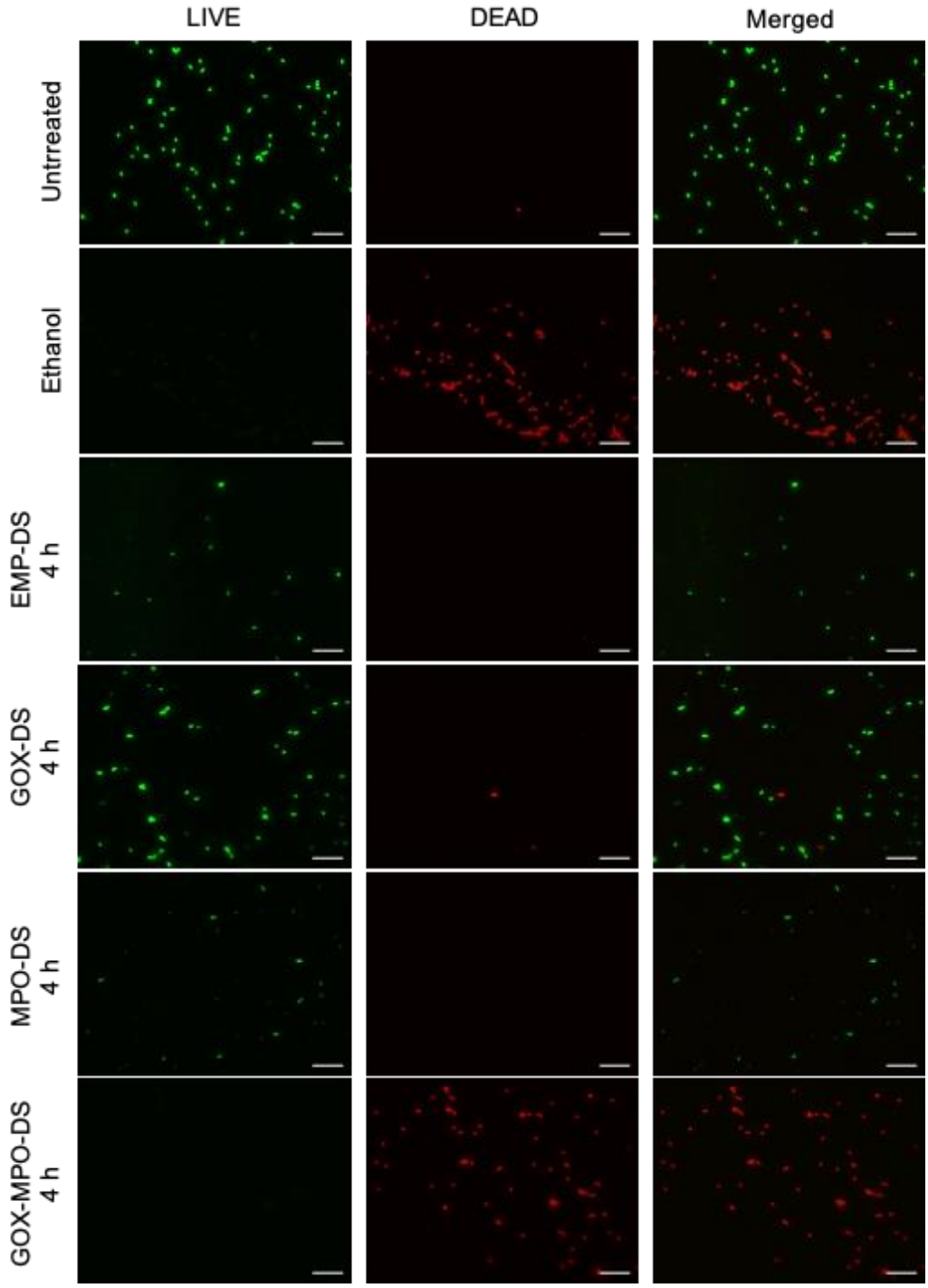

Supplementary Figure 24. LIVE/DEAD® fluorescence microscopy to demonstrate bactericidal effect of GOX-MPO-DS against *Pseudomonas aeruginosa*. All DS nanoreactors were incubated with glucose (10 mM) for 4 hours. Ethanol and untreated bacteria represent the positive and negative controls of bacterial killing. Scale bars = 10 µm.

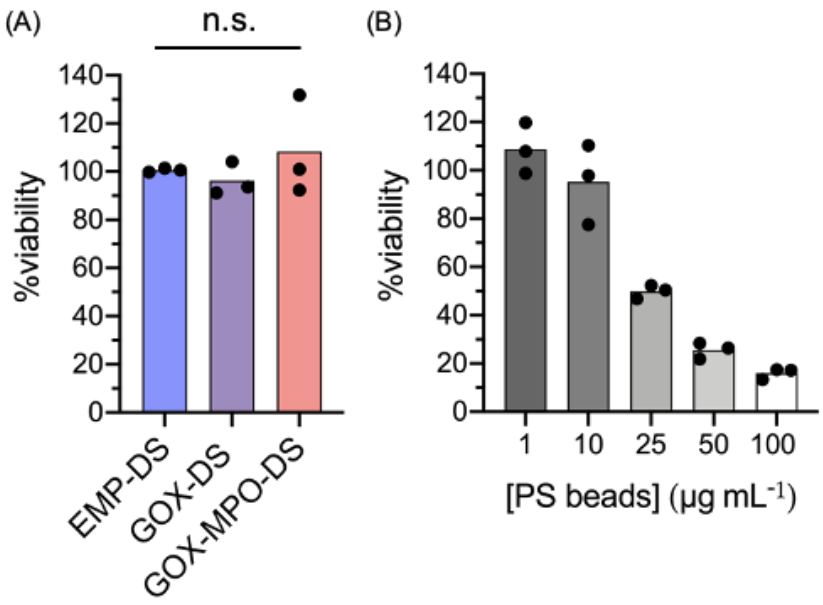

Supplementary Figure 25. Assessment of DS nanoreactor cytotoxicity against RAW 264.7 (macrophage) cells following 24-hour incubation in the presence of glucose (20 mM) and NaCl (103 mM). (A) Data for DS nanoreactors are mean ± SD (N = 3, n = 3). Dots represent the mean average of each biological repeat. Statistical significance was determined using a one-way ANOVA with Tukey's multiple comparisons test. $P < 0.05$ was considered to be statistically significant. (B) Data for PS beads are mean ± SD (N = 1, n = 3). Dots represent each technical repeat.

References

(1) Zhang, S.; Sun, H. J.; Hughes, A. D.; Draghici, B.; Lejnieks, J.; Leowanawat, P.; Bertin, A.; Otero De Leon, L.; Kulikov, O. V.; Chen, Y.; Pochan, D. J.; Heiney, P. A.; Percec, V. "Single-Single" Amphiphilic Janus Dendrimers Self-Assemble into Uniform Dendrimersomes with Predictable Size. *ACS Nano* **2014**, *8*, 1554–1565.

(2) Zhang, S.; Xiao, Q.; Sherman, S. E.; Muncan, A.; Ramos Vicente, A. D. M.; Wang, Z.; Hammer, D. A.; Williams, D.; Chen, Y.; Pochan, D. J.; Vértesy, S.; André, S.; Klein, M. L.; Gabius, H.-J.; Percec, V. Glycodendrimersomes from Sequence-Defined Janus Glycodendrimers Reveal High Activity and Sensor Capacity for the Agglutination by Natural Variants of Human Lectins. *J. Am. Chem. Soc.* **2015**, *137*, 13334–13344.

(3) Moore, J. S.; Stupp, S. I. Room Temperature Polyesterification. *Macromolecules* **1990**, *23*, 65–70.

(4) Movasaghi, Z.; Rehman, S.; Rehman, I. U. Raman Spectroscopy of Biological Tissues. *Appl. Spectrosc. Rev.* **2007**, *42*, 493–541.